Hindawi
Shock and Vibration
Volume 2023, Article ID 8966724, 19 pages
https://doi.org/10.1155/2023/8966724

Research Article

Design of Torsion Plate Energy-Absorbing Member and Analysis of Energy-Absorbing and Anti-Impact Characteristics

Jianzhuo Zhang,[1] Hao Guo,[1] Yonghui Xiao,[2] Yishan Pan,[2] Biao Jiang,[3] Shijie Su,[4] and Baojun Ni[1]

[1]*School of Mechanical Engineering, Liaoning Technical University, Fuxin 123000, China*
[2]*School of Physics, Liaoning University, Shenyang 110036, China*
[3]*Shandong Yankuang Intelligent Manufacturing Co., Ltd., Zoucheng 273500, China*
[4]*China National Coal Group Co., Ltd., Beijing 100120, China*

Correspondence should be addressed to Hao Guo; lntu_jxxy_gh@163.com

Received 6 January 2023; Revised 12 March 2023; Accepted 29 July 2023; Published 23 August 2023

Academic Editor: Desmond Adair

In order to effectively improve the impact resistance performance of the roadway anti-impact hydraulic support and reduce the loss caused by rock burst to a certain extent, a torsion plate energy-absorbing member was designed for using with the hydraulic column. By using theoretical analysis and numerical simulation methods and combining them with the parameters of the energy-absorbing characteristics evaluation index, single-factor tests were designed. Under the premise of constant impact velocity, the influence law of torsion angle, plate thickness, and fillet radius of the pressure plate on the energy-absorbing and anti-impact characteristics of energy-absorbing members were analysed. The results show that the deformation process and resistance trend of the torsion plate correspond to energy absorption. The resistance stability is high in the reaction force platform stage, and the energy increases linearly. With the increase of the torsion angle, the mean value of the reaction force increases, the fluctuation of the reaction force platform stage becomes more obvious, the specific energy absorption increases linearly, and the standard deviation reaches the minimum at 480°. Both the tensile length and the length of the reaction force platform stage increase continuously. With the increase of the plate thickness, the flatness of the torsion plate shows a trend of bad-good-bad, the mean value of the reaction force gradually increases, the specific energy absorption grows faster and then slower, and the tensile length and the length of the reaction force platform stage increase accordingly. With the increase of the fillet radius, the flatness of the torsion plate is better and the reaction force has a small improvement. The fluctuation of reaction force is most significant when the fillet radius is 2 mm, and the energy-absorbing member has the largest swing. The specific energy absorption is highest when the fillet radius is 2.5 mm, the standard deviation shows a tendency to develop firstly decreasing and then stabilising, the tensile length of the torsion plate decreases slightly, and the length of the reaction force platform firstly increases and then tends to stabilise. The torsion plate energy-absorbing member is a more ideal energy-absorbing and anti-impact member, which plays a positive role in the energy-absorbing and anti-impact of the hydraulic support.

1. Introduction

Mining dynamical disaster is an important factor affecting coal mining, which determines the production and workers' lives and safety. Among them, rock burst is one of the components of mining dynamical disaster [1–4]. Rock burst is a dynamic disaster caused by the sudden destabilization failure of coal and rock bodies such as underground working faces, roadways, and coal pillars [5, 6]. As the shallow coal seam is exhausted, the coal storage below 600 m in China accounts for more than 75% of the total storage, so it has become an inevitable trend to deep mining. However, with the increase of mining depth, the coal body will appear impact tendency, local stress concentration, coal and rock structure mutation and geological structure changes, and other multi-directional factors, resulting in frequent

occurrence of the rock burst phenomenon. Rock burst can cause a series of destructive phenomena such as rib spalling and roof falling, support destruction, roadway collapse, and facility destruction, and the frequency of rock burst in the roadway is higher than that in the mining face [7, 8], so effectively and reasonably mitigating the damage of rock burst on the support equipment and improving the integrity of the protection of the support equipment to the working zone are urgent problems to be solved.

Hydraulic support is an important support device for underground work, and its support effect determines underground production and workers' lives and safety. The hydraulic supports are equipped with different forms of safety valves. When the loading pressure exceeds the safety valve adjustment threshold, the safety valve opens automatically and the movable column falls steadily. This process can not only absorb energy but can also effectively provide displacement. However, the occurrence of rock burst is often instantaneous, and its power conversion time is less than the start time of the safety valve. Since the safety valve cannot be opened quickly, the pressure in the cylinder increases sharply and the support reaction force generated by the impact often exceeds the quasi-static load, which will cause the hydraulic column expansion, bending, and can even burst cylinder. Eventually the column is damaged, and the support effect is lost. Pan et al. [9] found that reasonably increasing the damping of the support equipment can reduce the acceleration response amplitude of the overlying rock blocks adjacent to the supporting system, calm the dynamic response of the rock block in a short time, and protect the support from damage. For this reason, they proposed a rigid-flexible coupling support method and a flexible energy-absorbing device is installed inside the support. When the load exceeds the load-bearing threshold of the energy-absorbing member, the energy-absorbing member actively gives way to absorb energy, providing a good time base for the activation of the safety valve. Indoor and field tests have proven that this method can reasonably mitigate damage to the support and the roadway from rock burst and ensure the integrity of support equipment.

At the present stage, the forms of energy-absorbing members used mainly include circular ring stacked type, circular ring expanded type, prefolded induced type, corrugated turned type, thick-walled split curl type, and foam filled composite structures. To this end, a lot of research has been conducted by scholars at home and abroad. Dai and Ma [10] modified the Singace stacking model to investigate the strain intensification effect, strain rate intensification effect, and temperature intensification effect on the energy absorption under impact loading based on the J-C eigenstructure equation. Tang et al. [11] designed a hexagonal thin-walled member applied to the top beam of the support. The structure had a stable failure mode, constant reaction force, and high stroke efficiency. It had a good energy-absorbing effect and practical application value. Wang et al. [12] carried out numerical simulation and experimental research on circular tubes with one-shaped ribs, cross-shaped ribs, and *Y*-shaped ribs, respectively. They found that the deformation of the one-shaped ribs was irregular, the cross-shaped ribs had the phenomenon of cracking and deflection, and the deformation of *Y*-shaped ribs was relatively regular. Luo et al. [13] proposed the indefinite preprocessing of the expansion ring to improve energy-absorbing efficiency and reduce fluctuations for the energy-absorbing characteristics of thin-walled aluminum tubes under plastic deformation under quasi-static action. Xiao et al. [14] verified the energy-absorbing effect of prefolded energy-absorbing members by structural optimization, reliability analysis, and field tests. Zhang et al. [15] designed a straight bellows outturned energy-absorbing member, used the energy method to theoretically derive its deformation resistance, and combined with numerical simulation to improve the member. The improved energy-absorbing member has constant resistance characteristics, and the theoretical calculation and numerical simulation results reach match. Qi et al. [16] studied the failure mode and energy-absorbing characteristics of an axisymmetric conical multicellular thin-walled square tube under different impact angles and fitted analytical formulas that can be used to predict specific energy absorption and impact peak force under oblique impact, which provided reference and basis for such structural design.

There are various forms of energy-absorbing members, but there are various problems, such as thin-walled circular ring energy-absorbing members, which have fluctuations in the reaction force during axial collapse, uncertainty in the location of the yield point, Euler instability, and other phenomena. Prefolded induced energy-absorbing members have improved compared to circular ring members, but there is still a significant "*W*" fluctuation effect. The inversion type member has a weak point tearing phenomenon during the actual force deformation process. The splitting curl type of energy-absorbing member has various forms of splitting in its middle section, which cannot develop according to the prescribed trend. The foam metal type of energy-absorbing member has high cost and low energy-absorbing efficiency. In view of the abovementioned problems of energy-absorbing members, in this study, an energy-absorbing member based on a torsion plate was proposed, which absorbed dissipated impact energy by torsional deformation of the torsion plate according to the prescribed trend, and it improved the anti-impact performance of the support. It is simple to process, easy to install, and easy to carry. It has stable reaction force and excellent energy-absorbing effect. It can be reasonably matched with the number of installations based on the requirements, according to the single-factor test method, to study its energy-absorbing and anti-impact characteristics.

2. Design and Evaluation of Energy-Absorbing Members

2.1. Requirements for Energy-Absorbing Members and Evaluation Parameters of the Anti-Impact Support. When there are no dynamic disasters in the mine roadway, the support system often bears quasi-static loads. But when rock burst occurs, due to the energy accumulated in the coal and rock

body being transferred to the support system in a short time, the support members are subjected to the instantaneous impact or large load. So, according to the actual working conditions, the design and selection of energy-absorbing members should meet the following requirements:

① The member should have a more reasonable flexural critical resistance F_{max}: the working conditions of the member mainly include quasi-static load and dynamic load. Under the action of quasi-static load or small impact dynamic load, the member should have a better bearing capacity. When the impact load reaches the critical resistance, it rapidly deforms and absorbs energy, achieving the protection of the member. The threshold value should theoretically be between the working resistance of the column and the impact damage load of the column and other members. According to the relevant national standards, the value should be between 1 and 1.5 times of the working resistance of the column.

② Larger energy-absorbing capacity and higher reaction force: the energy-absorbing process is an irreversible energy dissipation mode. This process dissipates rapidly the energy released by the rock burst in other forms of energy such as deformation energy and heat energy to complete the protection effect on the hydraulic support. The total energy E and the mean value of the reaction force F_{mean} are as follows:

$$E = \int_0^x F(s)ds,$$
$$F_{mean} = \frac{E}{x}. \tag{1}$$

Here, $F(s)$ is the value of the different support reactions of the energy-absorbing member during the load-bearing process; x is the displacement during the deformation of the energy-absorbing member.

③ The energy-absorbing member should have a long let-off stroke: on the one hand, the long let-off stroke can improve the effective energy absorption, and on the other hand, it can also provide the hydraulic support with the larger let-off energy consumption space and the longer let-off time, which also provides a guarantee for the effective opening of the safety valve. The effective let-off stroke is the distance reached when the reaction force increases to the initial peak F_{max} in the process of deformation of the member.

④ High specific energy absorption: specific energy absorption refers to the ratio of the total amount of energy absorbed under load to the mass of the member. That is the efficiency of energy absorption per unit mass, the greater the *SEA* reflects, the better the energy absorption effect and the opposite is the worse the effect.

$$SEA = \frac{E}{m}. \tag{2}$$

⑤ Stable reaction force: energy-absorbing members should be able to provide a relatively smooth buffer protection to the support system during the process of energy absorption of collapse.

$$\sigma = \sqrt{\frac{1}{x_2 - x_1}\int_{x_1}^{x_2} \left(F(s) - F_{mean}\right)^2 ds}. \tag{3}$$

Here, x_1 and x_2 are the initial and end positions of the deformation process of the energy-absorbing member, respectively.

⑥ Longer reaction platform length: energy-absorbing members should have a longer reaction platform length s, to increase the absorption of the members.

⑦ The deformation of the energy-absorbing members is repetitive and controllable, under conditions of varying structural parameters in order to adapt to different working environments and be easy to install.

2.2. Design of Torsion Plate Energy-Absorbing Members. The design of the torsion plate energy-absorbing member aims to "straighten" the torsion plate by means of a mobile pressing plate to restore the torsion plate to a nearly straight state, through the process of the plastic deformation of the torsion plate to complete the energy absorption. The member consists of a deformation torsion plate, a fixed box, and a mobile pressing plate. The torsion plate is pretreated with a straight steel plate, and the torsion angle is set to deform the plate in advance. In order to achieve the fixation of the energy-absorbing member, the end of the torsion plate is welded with a "*T*" shaped tab end, while the lower end of the fixed top plate of the outer box is welded with a "*T*" shaped slot. The mobile pressing plate is a steel plate with a certain thickness, and a rectangular hole matching the size of the "*T*" tab end is opened at the centre of the steel plate. As the border of the rectangular hole is right angle, in the process of contacting with the torsion plate, the smaller contact area will damage the pressing plate member to a greater extent, so the lower port boundary of the rectangular hole is rounded, as shown in Figure 1. The assembly diagram of the energy-absorbing member is shown in Figure 2. The torsion plate deformation form is stable, and the deformation state of the whole deformation process is consistent, so in the deformation process it can achieve a stable reaction force effect. Its ideal deformation process is shown in Figure 3. The torsion plate is simple to process and is easy to carry and assemble, and the number of torsion plates can be adjusted according to the load required to achieve the energy-absorbing effect. Only the core member, the torsion plate, needs to be replaced during replacement. This structure can be used in various positions, such as above the top beam of the hydraulic support, at the side shields, etc., all of which can effectively play a role in energy absorption and have a wide range of applications. In the design

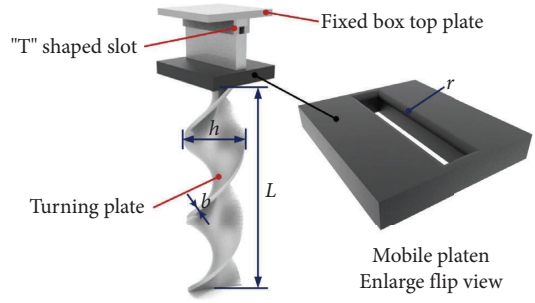

Figure 1: Torsion plate energy-absorption member.

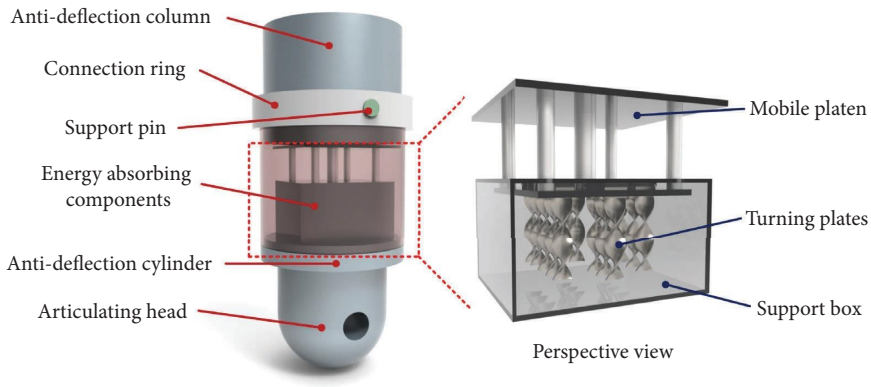

Figure 2: Energy-absorption device assembly diagram.

Figure 3: The ideal deformation process of the torsion plate.

of the member, the total length of the torsion plate is defined as L, the cross-sectional length is defined as h, the cross-sectional width, i.e., the thickness of the torsion plate is defined as b; the torsion angle is defined as θ. The torsion angle is the angle between the edge line of the bending section at the beginning of the plate and the end of the bending section; the fillet of the pressing plate port is defined as r. The initial structural parameters are defined in Table 1.

Table 1: Initial structural parameters of the energy-absorbing member.

L (mm)	h (mm)	b (mm)	θ (°)	r (mm)
200	50	5	480	3

3. Theoretical Analysis of Torsion Plate Energy-Absorbing Anti-Impact Members

As shown in Figure 4, this is a side view of the energy-absorbing member, where Figure 4(a) is the initial position of the energy-absorbing member, and Figure 4(b) is the initial contact position between the pressing plate and the torsion plate. Now, taking the centre of the initial deformation position of the torsion plate as the coordinate origin, along the axial downward direction as the X-axis, along the thickness of the torsion plate cross-section direction as the Y-axis, along the length of the torsion plate cross-section direction as the Z-axis, establishing the coordinate system as shown in the figure. The amount of torsion plate drop is Δx. The torsion plate extends downwards in a spiral shape so that in the Y and Z directions, the centreline extension of the torsion plate obeys the sine curve function and the cosine curve function, where the total length of the torsion plate is L and the torsion angle is θ.

Therefore, its centreline extension of the torsion plate in the Y direction is

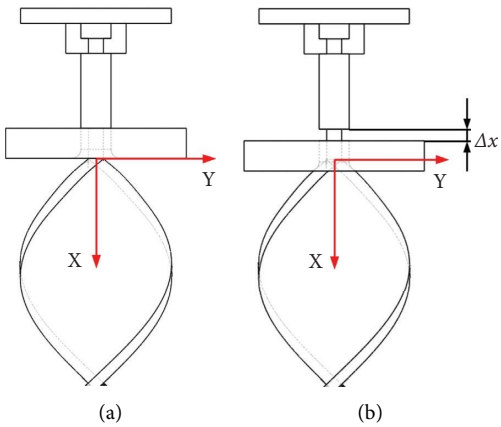

Figure 4: Side view of the energy-absorbing member.

$$f(x) = \frac{h}{2}\sin\left(\frac{\pi\theta}{180^\circ \cdot L}x\right). \tag{4}$$

Similarly, the centreline extension of the torsion plate in the Z direction is

$$f(x) = \frac{h}{2}\cos\left(\frac{\pi\theta}{180^\circ \cdot L}x\right). \tag{5}$$

As shown in Figure 5, the BD section is the fillet section of the pressing plate. When the pressing plate touches the torsion plate, the two intersect at the point O_2, and at this time, the coordinate of the O_2 point is $(x, h/2\sin((\pi\theta/180^\circ \cdot L)x) + b/2)$. The pressing plate is tangent to the torsion plate at the intersection position, and their slopes are the same. Taking the initial position of the pressing plate fillet B as the origin, to solve the slope of the BD section, t is the length of the BD section from the transverse coordinate of point B. So, the slope of the BD section of the pressing plate is as follows:

$$f'(t) = \frac{t}{\sqrt{r^2 - t^2}}. \tag{6}$$

Torsion plate slope:

$$f'(x) = \frac{\pi\theta h}{360^\circ \cdot L}\cos x. \tag{7}$$

When the two are in contact, the angle between the tangent line and the horizontal direction is α. Based on the two-dimensional relationship, we know that

$$\begin{cases} \mathrm{CD} = r - r \cdot \sin\alpha = r(1 - \sin\alpha), \\ \mathrm{AB} = r - r \cdot \cos\alpha = r(1 - \cos\alpha). \end{cases} \tag{8}$$

The energy absorption of the torsion plate deformation follows the law of conservation of energy. Due to the complex deformation of the torsion plate structural members, the force analysis is more difficult, so the theoretical inversion of its support reaction force is based on the law of conservation of energy. The ratio of the thickness of the torsion plate member to the total length of the plate is within 0.01 to 0.2, so it is a thin plate member [17, 18]. Based on the

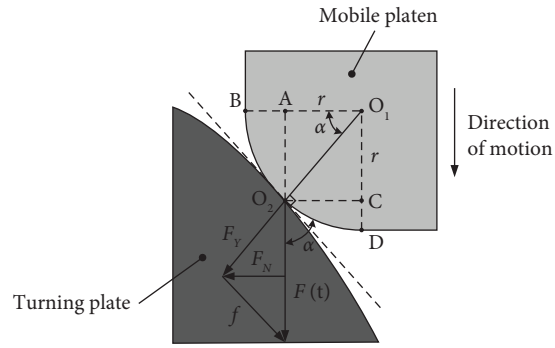

Figure 5: Torsion plate-pressing plate contact diagram.

thin film comparison principle, the plates follow the continuity assumption, the homogeneity assumption, and the isotropy assumption in terms of material and Kirchhoff's law in terms of deformation [19, 20]. The plate is transformed into a predetermined state by torsion on the basis of initial flatness. In the calculation of the torsion of a rectangular plate, when the boundary conditions are $x = \pm b/2$, $y = \pm h/2$, the boundary stress function satisfies $\psi_b = 0$. But at this time, the gradient function of Poisson's equation $\nabla^2\psi = -2G\varphi$ is not satisfied. It is difficult to determine the torsional stress function under this condition, so the Poisson equation is first calculated as a special solution and transformed into the Laplace equation [21–24], based on which the special solution is calculated as

$$\psi(x, y) = \psi_0(x, y) - G\varphi\left(y^2 - \frac{b^2}{4}\right). \tag{9}$$

For plate side boundary conditions $\psi_b = 0$, the boundary conditions need to be satisfied:

$$\begin{cases} \psi_0\left(\pm\dfrac{b}{2}, y\right) = G\varphi\left(y^2 - \dfrac{b^2}{4}\right) x = \pm\dfrac{b}{2}, \\ \psi_0\left(x, \pm\dfrac{h}{2}\right) = 0 \quad y = \pm\dfrac{h}{2}. \end{cases} \tag{10}$$

The plate cross-section is symmetrical about the axes X and Y, so the torque M is antisymmetric about the axes, and substituting the above equation gives

$$\frac{X''}{X} = -\frac{Y''}{Y} = \lambda^2. \tag{11}$$

By Laplace transform, it follows that

$$\begin{cases} X = A\cosh\lambda x + B\sinh\lambda x, \\ Y = C\cos\lambda x y + D\sin\lambda y. \end{cases} \tag{12}$$

The linear superposition of the special solutions gives the stress function general solution as

$$\psi_0(x, y) = \sum_0^\infty A_n \cosh\frac{(2n+1)\pi}{b} x \cos\frac{(2n+1)\pi}{b} y. \tag{13}$$

The expression of the stress function is

$$\psi(x, y) = \sum_0^\infty (-1)^{n+1} \frac{8b^2 G\varphi}{(2n+1)^3\pi^3} \frac{2\cosh\lambda_n x}{\cosh\lambda_n a} - G\varphi\left(y^2 - \frac{b^2}{4}\right). \tag{14}$$

At this point, the boundary torque of plate deformation is

$$M = 2\iint_S \psi dx\, dy = \frac{1}{3} Gb^3 h\varphi - \frac{129Gb^4\varphi}{2\pi^5} \sum_0^\infty \frac{1}{(2n+1)^5} \tan\lambda_n \frac{h}{2}. \tag{15}$$

It is calculated through its maximum point of rated force, the torsion angle per unit length and the maximum torsional shear stress are, respectively,

$$\varphi = \frac{M}{Gb^3 hk}, \qquad \tau_{\max} = \frac{M}{b^2 h\alpha}. \tag{16}$$

When the torsion plate changes from the initial state to the torsion state, the point of action of the external force acts on the boundary of = ± h/2. The deformation force is

$$F_b = \frac{M}{h}. \tag{17}$$

During the process of the torsion deformation of the torsion plate, its axial pressure load work is all converted into plastic deformation work. Considering that the plastic deformation of the torsion plate is mainly divided into two parts, the first part is the torsion work of the torsion plate cross-section and the second part is the torsion plate axial tensile work. According to the law of conservation of energy, we have

$$dW_F = dW_A + dW_B, \tag{18}$$

where dW_F is the axial pressure load work increment; dW_A is the torsion energy increment of the torsion plate; dW_B is the increment of tensile work on the torsion plate by frictional action. The total work of axial pressure load is

$$dW_F = F(t)dL, \tag{19}$$

where $F(t)$ is axial pressure variable loads; dL is the length of axial pressure action. The total work of torsion of the torsion plate is as follows:

$$dW_A = 2 \times F_N(t) \times dL, \qquad M = F_N r(h), \tag{20}$$

where $r(h)$ represents the torsion radius of the torsion plate at different positions. The torsion radius will change position as the torsion plate deforms:

$$dW_A = \int_0^L 2 \times \frac{Ghb^3 k\theta\pi}{180^\circ r(h)\sin 2\alpha} dL. \tag{21}$$

Total work of friction stretching:

$$dW_B = \mu \int_0^L 2 \times \frac{Ghb^3 k\theta\pi}{180^\circ r(h) 2\sin\alpha} dL,$$

$$dW_F = \int_0^L \frac{Ghb^3 k\theta\pi}{90^\circ r(h)\sin 2\alpha} dL + \mu \int_0^L \frac{Ghb^3 k\theta\pi}{90^\circ r(h) 2\sin\alpha} dL = \left(\frac{1}{\sin 2\alpha} + \frac{\mu}{2\sin\alpha}\right) \int_0^L \frac{Ghb^3 k\theta\pi}{90^\circ r(h)} dL. \tag{22}$$

The pressure plate in the process of downward movement on the torsion plate produces friction so that the torsion plate produces axial tensile load, and its tensile length is Δl. During the design and study of the torsion plate, Δl should be reduced as much as possible so that the reaction force is more used in the torsion process of the torsion plate members, while the reduction of the possibility of the torsion plate is pulled off, where the torsion plate tensile length is

$$\Delta l = \sum_{i=1}^n \frac{\mu F_N l_i}{\cos\alpha E_i A_i}. \tag{23}$$

4. Simulation Study of Torsion Plate Energy-Absorbing Anti-Impact Members

4.1. Simulation Parameter Setting. The study used the ABAQUS dynamic display algorithm to simulate the torsion plate straightening and flexure process and defined the torsion plate material as Q235 and the pressing plate material as 45 Steel. Both parameters are shown in Table 2. The torsion plate is the main deformation member, in the process of plastic deformation subjected to compressive and tensile stresses, the deformation is a large deformation, so the stress intensification stage is considered. In the process of

Table 2: Material properties.

Materials	Density (kg/m^3)	Young's modulus (GPa)	Poisson's ratio	Yield stress (MPa)
Q235	7830	210	0.274	235
45Steel	7890	209	0.269	355

defining the plastic properties of Q235, the hardening mode is chosen to be isotropic. The yield strength of Q235 is 235 MPa, the tensile strength is 441–550 MPa, the upper limit of the real stress of the material is taken to 515 MPa, and the real stress-strain values are written in Table 3. The analysis and calculation are performed by using the explicit dynamic analysis method, and the time length is set to 0.05 s. The tangential behaviour of the interaction is set as penalty friction, and the friction coefficient is 0.25. The normal behaviour is hard contact, and the interaction type is defined as generic contact. The boundary of the torsion plate member is defined as completely fixed. The pressing plate is restricted to all degrees of freedom except for axial movement, the distance of negative motion of the pressing plate along the Y-axis is 200 mm, and the amplitude is in the form of linear growth. Both the torsion plate and the pressing plate are meshed with the hexahedral structured mesh, which can effectively improve the efficiency and accuracy of the simulation. The mesh cell type is Explicit-C3D8R eight-node linear hexahedral cells for the advanced algorithm of hexahedral mesh cell division. The mesh size is set to 0.1 mm, which can effectively ensure that the mesh layer at each position of the global structure is not less than 4 and enhance the accuracy of numerical simulation. After the mesh checking, the total number of meshes is 108096, the number of analysis errors is 0, the number of warnings is 3.75%, and the mesh division effect is good.

4.2. Simulation Results and Analysis

4.2.1. Deformation Process and Stress Analysis. As shown in Figure 6 is the torsion plate energy-absorbing member deformation stress cloud diagram. From the figure, it can be seen that the pressing plate will move with a constant impact velocity when it is not in contact with the torsion plate. When the pressing plate contacts the torsion plate, the torsion plate boundary begins to occur as initial deformation, and at this time, the torsion plate is subjected to the stress of 318.4 MPa. As the pressing plate continues to move down, the torsion plate is reverse torsion, and at this time, the stress rapidly increases to 515 MPa near. After the deformation of the initial section of the torsion plate, the effect of the subsequent section is the same as that of the initial section. From Figures 6(c)–6(e), it can be seen in the right part of the torsion plate in the centre line direction that there is an obvious scratch phenomenon and the scratch point is not in the right side of the torsion plate. Due to the deformed part being affected by the internal material elasticity recovery ability, after becoming nearly rectangular, it will continue to realise torsion variation and the torsion plate from left to right is approximately an sinusoidal wave. So, the lower end of the torsion plate begins to gather inward at the contact position with the pressing plate. As shown in Figure 7, at this time, the internal stress of the torsion plate gradually increases. When the pressing plate is lowered to about 60 mm, the deformation of the torsion plate remains consistent, and no cohesion occurred at the location of the scratches. It is proved that after 60 mm, the stress does not occur as a large step phenomenon and the deformation of the torsion plate is stable until moved to the specified position. During the pressing plate moving down, the pressing plate in addition to make the torsion plate occur plastic deformation to reverse torsion, due to the relative movement of the two will produce friction, the friction will produce the downward tensile stress on the torsion plate to produce tensile plastic deformation of the torsion plate. At the end of the pressing plate stroke, the part of the torsion plate is not involved in energy absorption. As shown in Figures 6(a) and 6(e), the distance difference is 36.54 mm in the figure. The tensile plastic deformation is within the tensile limit of the material, so the material will not be pulled off due to longitudinal stretching, and the remaining part of the length which is not involved in the torsion is still able to continue to participate in the energy absorption. As the torsion length of the torsion plate increases, the stress in the middle section decreases, and only in the section that contacts the pressing plate, the stress value is higher and remains stable. The top part of the torsion plate is welded to the "T" shaped tab, and the stress at the weld is less. This position can effectively withstand the stress caused by the deformation and ensure that the end is not pulled off.

Table 3: Q235 true stress strain value.

Real stress σ_t (MPa)	Real strain ε_t
235	0
281	0.0235
329	0.0474
409	0.0935
427	0.1377
515	0.1377
515	0.18

4.2.2. Reaction Force and Energy. The reaction force-energy-displacement curve of the deformation process of the torsion plate energy-absorbing member is shown in Figure 8. From the figure, it can be seen that the trend of resistance change during the deformation of the torsion plate by the downward pressure of the pressing plate can be roughly divided into four stages. At the first stage, resistance increases to 17.5 kN at the initial stage of deformation. During the process, the pressing plate is elastic deformation and the reaction force rises linearly and rapidly. The second stage is the initial plastic deformation stage. At the stage, the material of the torsion plate is plastic deformation, and the material occurs

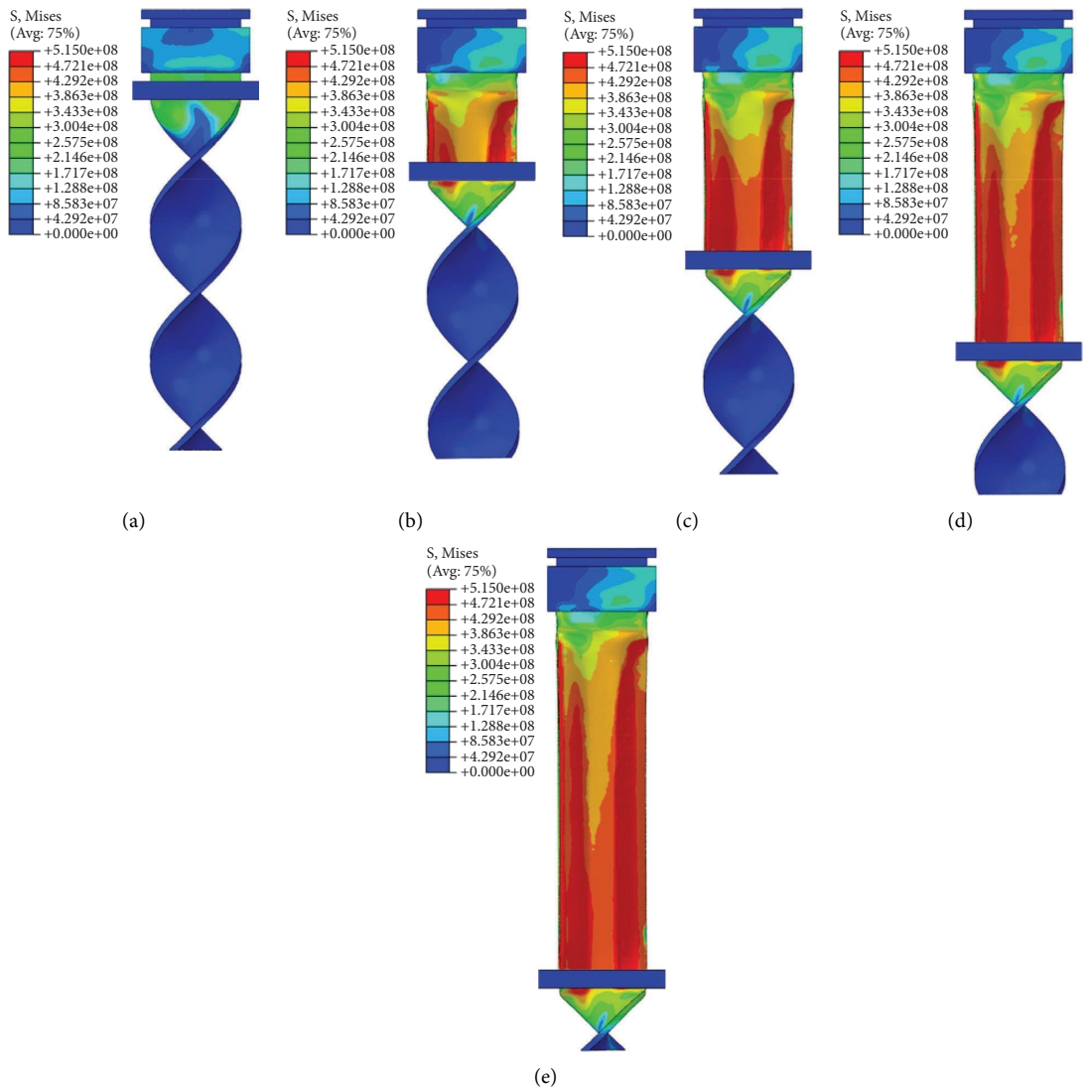

Figure 6: Deformation stress cloud diagram of torsion plate energy-absorbing member. (a) Contact point. (b) Force stability. (c) 100 mm. (d) 150 mm. (e) 200 mm.

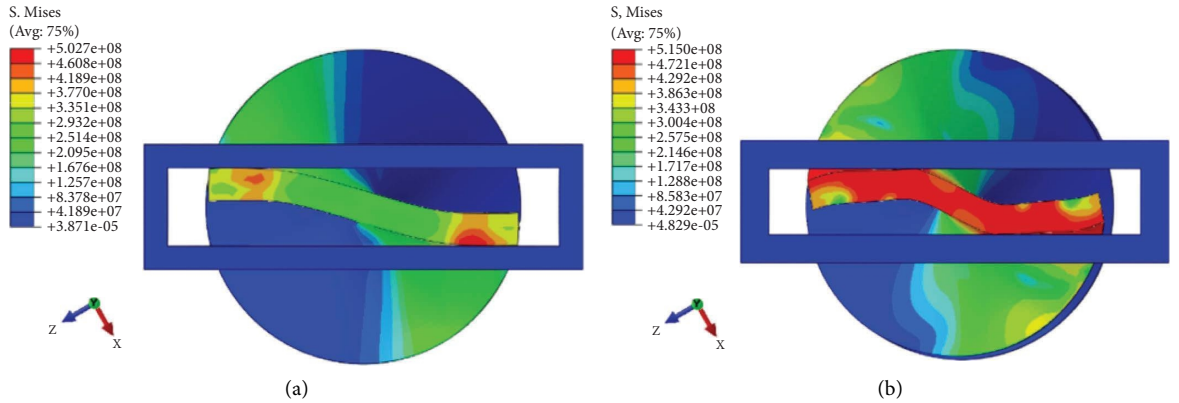

Figure 7: The contact position of the pressure plate and the torsion plate. (a) Initial contact section location. (b) Process contact section location.

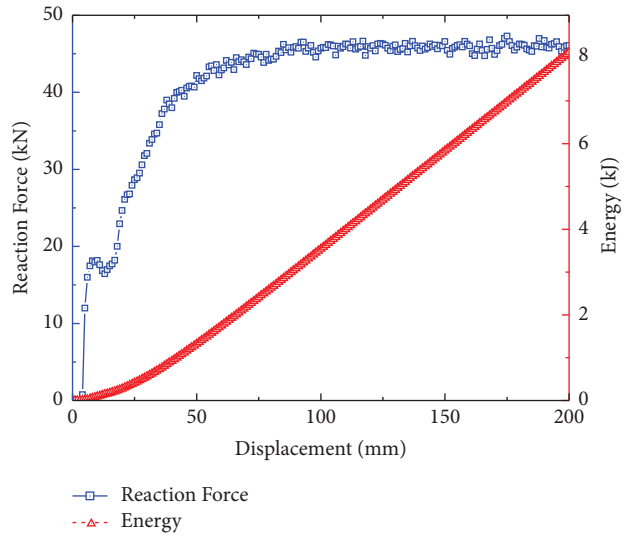

Figure 8: Reaction force-displacement curve.

yielding, so the support reaction force remains in the stable interval. This stage guides the lower end of the torsion plate to have a stable deformation tendency and plays a role in guiding the deformation. When the initial deformation point passes through the pressing plate, the initial stage of deformation is completed. At the third stage, the pressure gradually increases from 18.2 kN to 45.0 kN. This stage represents the inward convergence of the contact points of the torsion plate and the pressing plate. The deformed part generates a reverse torque on the undeformed part, and the contact point gradually moves inward. Due to the contact point moving inward, the torsion deformation bending moment of the torsion plate decreases, so the external force of this stage gradually increases. At the same time in the process, the material shows a stress intensification phenomenon as the stress increases, so there will be a reaction force climbing stage. The fourth stage is the stable deformation stage of the torsion plate. The reverse torque generated by the deformed part remains constant during this stage, so the position of the contact point between the undeformed part and the pressure plate is stabilised around the same position. At this time, the deformation torque of the torsion plate remains unchanged, so the support reaction force of the torsion plate deformation remains stable. When the pressure plate continues to move down, the resistance of the torsion plate deformation remains unchanged until the movement of the pressure plate stops. The energy-absorbing member can produce a stable support reaction force, the fluctuation of the support reaction force is small, and there is no obvious pressure peak point. Therefore, the energy-absorbing performance of this member is reasonable, and it is an ideal energy-absorbing member. During the design and selection of the energy-absorbing member at the bottom of the hydraulic column, it is ensured that the working resistance of the hydraulic support should be in the stage of the reaction force climbing of the energy-absorbing member. When the value of the reaction force is determined, the torsion plate energy-absorbing member can be pressed down to this position in advance, which ensures that the reaction force platform value of the energy-absorbing member is stabilised at around 1.5 times the working resistance of the support and achieves the optimal energy-absorbing effect. The energy absorption is divided into three stages. The first stage is the initial deformation stage of the torsion plate, which corresponds to 6~16 mm. The resistance has only a small climb, and the energy absorption increases almost linearly. At the second stage, the deformed torsion plate is torsionally deformed by the torque of the upper torsion plate which makes the contact point between the torsion plate and the pressure plate move inward. With the moving distance of the pressure plate increasing, the distance of inward movement of the contact point increases and the torsional bending moment decreases, which makes the change of resistance rise continuously. As the downward pressure distance increases, the absorbed energy increases nonlinearly. The third stage is the stable stage of the torsion plate deformation. The position of the contact point remains constant, the torsional torque remains constant and the resistance of the member remains constant. With the compression distance increasing, the energy-absorbing capacity increases linearly.

4.2.3. Evaluation Indicators. Energy absorption evaluation indicator parameters are shown in Table 4. The mean load accounts for 85.83% of the maximum load, the total absorbed energy is 8.13 kJ, and the specific energy absorption is 20.72 kJ/kg. In this study, the dynamic characteristics of the torsion plate are mainly considered. Therefore, during the analysis of the specific energy absorption, only the mass of the main body of the torsion plate is taken into account for the calculation and analysis, and the mass of the other members of the energy-absorbing device under the assembly conditions is not considered. The value of specific energy absorption is relatively significant compared to other forms of energy-absorbing members. The residual amount of the end of stroke section is 36.54 mm, which is 18.27% of the total original length. In this study, the fluctuation of the reaction force platform stage of the torsion plate energy-absorbing member is analysed, and the standard deviation of the support reaction force of the 100 mm~200 mm length is taken as the evaluation indicator of the fluctuation of the support reaction force of the plate. The standard deviation of the reaction force in the platform stage is 490.8 N. The simulated pseudostrain energy is 731.05 J, accounting for 8.99% of the total energy, which does not exceed 10% of the total energy, and its fluctuation is small.

5. Single Factor Variable Studies

The structural parameters of the energy-absorbing members are important influencing factors that affect the impact energy-absorbing characteristics of the structural members, and they are also an important basis for the selection of the energy-absorbing members. In this section, the mean value of reaction force, swing displacement, energy absorption, specific energy absorption, torsion plate tensile length,

Table 4: Energy absorption evaluation indicator parameters.

F_{max} (kN)	F_{mean} (kN)	E (kJ)	SEA (kJ/kg)	Δl (mm)	σ (N)
47.3	40.6	8.13	20.72	36.54	490.8

standard deviation of platform reaction force, and length of reaction platform stage are used as the measurement indexes to investigate the influence of variation of torsion angle θ, plate thickness b, and fillet radius r on the impact energy-absorbing characteristics of structural members. The design tests are shown in Table 5.

5.1. Effect of Torsion Angle on the Impact Energy Absorption Characteristics. Under the conditions of impact velocity of 4 m/s, total length of 200 mm, plate thickness of 5 mm, and fillet radius of 3 mm, the simulation studies were carried out for torsion plates with torsion angles of 240°, 360°, 480°, 600°, and 720°. As shown in Figure 9 for different torsion angle conditions under the pressure plate displacement 200 mm energy-absorbing members stress cloud diagram. From the figure, it can be seen that when the torsion angle is small, such as 240° and 360°, after the pressure plate is pressed, the torsion plate appears to continue to rotate after the flattening phenomenon. As the torsion angle decreases, the more obvious the rotational phenomenon after the pressure plate is pressed. This phenomenon is due to when the torsion angle is small, in its horizontal cross-section of the deformation moment is small, only in the torsion plate and pressing plate contact position has occurred plastic deformation, and the torsion plate in the middle of the position of the stress is small. It did not occur obvious plastic deformation, still has the elastic capacity. Therefore, after the deformation at both ends, the middle section has the performance of maintaining the original state, and by the role of the bending moment of the pressure plate below to restore the torsion, the middle section has no obvious deformation. With the increase of the torsion angle, the pressure plate in the torsion of the torsion plate will produce a greater torque. This torque causes plastic deformation in the contact section between the torsion plate and the pressing plate. After the press plate has moved, the torsion plate that has deformed plastically above it loses its ability to return to its original state, and therefore, no recovery torsion occurs. In addition, when the torsion angle reaches 600°, the torsion plate swings significantly when the press plate is pressed down. This phenomenon is due to the fact that the torsion plate is subjected to excessive stress concentration at a certain point, which causes the plate to develop a stage of scratches. The torsion plate gives way in the direction of the other side and then repeats the phenomenon on the other side. The continuous overlapping of this phenomenon causes the torsion plate to swing. The swinging phenomenon causes the magnitude of the reaction force to fluctuate, which is not conducive to the yielding of the system and should be avoided as much as possible.

The reaction force-displacement curves of the energy-absorbing members under different torsion angles are shown in Figure 10. As can be seen from the figure, each energy-absorbing member has elastic deformation stage, yield deformation stage, reaction force raising stage, and platform stage. There is no obvious peak pressure point or resistance drop in the members, and the platform stage is longer and smoother. As the torsion angle increases, the reaction force reaches the platform stage faster, and the mean values of reaction force under the five conditions are 8.99 kN, 24.82 kN, 40.58 kN, 47.86 kN, and 50.91 kN, respectively. When the torsion angle is 240°, the plate does not undergo all plastic deformation during torsion. It entered the platform stage directly after the elastic deformation stage. The platform reaction force is stable, but the value is too small and the support ability is poor. Torsion angle in 360° and 480° under the two conditions of the reaction force without obvious fluctuations, more stable, and with the increase of the torsion angle reaction force gradually increased. When the torsion angle reaches 600°, the reaction force platform stage appears as an obvious fluctuation phenomenon. Considering this phenomenon is due to the increase in the torsion angle, the counterforce is elevated, and its cross-section torsion force F_N increases, while the pressure plate will scratch the torsion plate in the process of moving down. Torsion plate side of the plastic deformation gives way to make the nonplastic deformation section swing, resulting in the appearance of the stage of the scratch, the reaction force with the swing of the torsion plate fluctuation phenomenon, fluctuation phenomenon is not conducive to the effective support of the torsion plate.

Table 5: Test design.

Test number	Torsion angle θ (°)	Plate thickness b (mm)	Fillet radius r (mm)
1	240	5	3
2	360	5	3
3	480	5	3
4	600	5	3
5	720	5	3
6	480	3	3
7	480	4	3
8	480	6	3
9	480	7	3
10	480	5	2
11	480	5	2.5
12	480	5	3.5
13	480	5	4

As shown in Figure 11, the energy absorption curves of the energy-absorbing members at different torsion angles, from the figure can be seen, the final energy absorption of the five groups of members are 1.80 kJ, 4.98 kJ, 8.13 kJ, 9.59 kJ, and 10.8 kJ. In the first half of the stage, with the increase of the torsion angle, the energy absorption of the members gradually increases. When the torsion angle exceeds 480°, torsion plate reaction force fluctuations occur and the trend in energy growth has slowed down, but it can still be linearly increased.

The bottom surface centre point along the torsion plate cross-section width direction swing displacement is shown in Figure 12. As can be seen from the figure, when the torsion angle of 240°, the torsion plate there is only a very

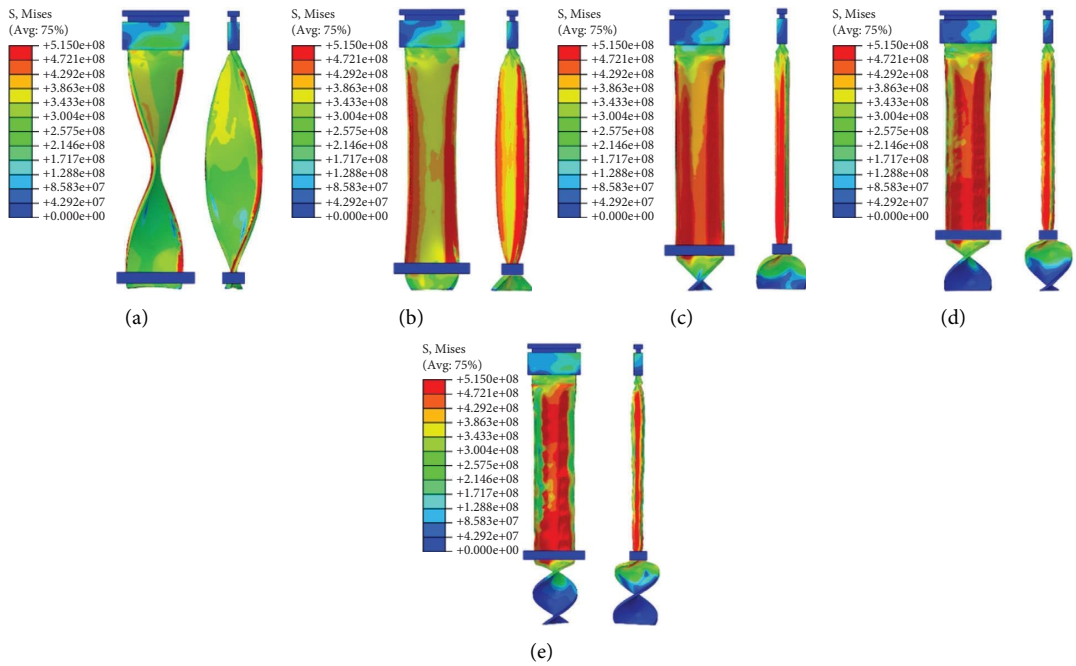

Figure 9: Stress cloud diagram of members with different torsion angles. (a) $\theta = 240^{\circ}$. (b) $\theta = 360^{\circ}$. (c) $\theta = 480^{\circ}$. (d) $\theta = 600^{\circ}$. (e) $\theta = 720^{\circ}$.

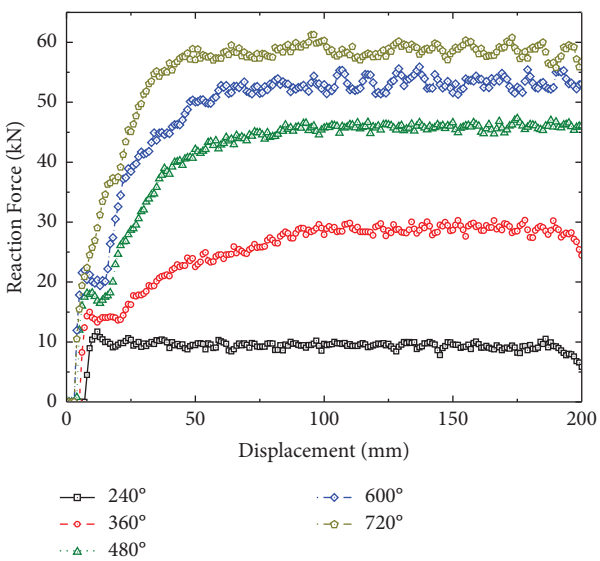

Figure 10: Reaction force-displacement curves of members with different torsion angles.

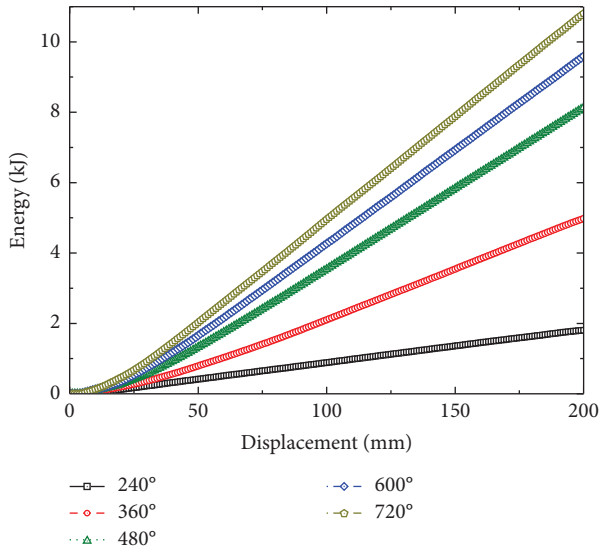

Figure 11: Energy absorption characteristic curves of members with different torsion angles.

small swing displacement of 0.69 mm, and in the early swing after the tendency to stabilise, the position does not change. With the increase of the torsion angle, the torsion plate member of the swing phenomenon is obviously strengthened, 360° of the maximum swing amplitude of 1.03 mm, 480° of the maximum swing amplitude of 1.40 mm, both in the preswing after the stabilisation. When the torsion angle reaches 600° or more, torsion plate deformation appears as an obvious stage scratch phenomenon, plate side of the stress concentration will give way to the other side so as to repeat the phenomenon of swing, and with the increase of the torsion angle, the swing amplitude rises significantly. The maximum swing amplitude of 600° and 720° is 3.31 mm and 3.99 mm, respectively. The increase in the amplitude of the swing has a negative effect on the stability of the energy absorption.

The standard deviation of reaction force and specific absorption energy curves at different torsion angles are shown in Figure 13. As can be seen from the figure, with the increase of the angle, the *SEA* gradually increases and slows down. The change trend of specific absorption energy is the same as that of energy. As the torsion angle increases, the reaction force increases, but the swing trend is obvious, so the energy increases slower and the *SEA* increases slower as well. The standard deviation of the reaction force is a nonlinear

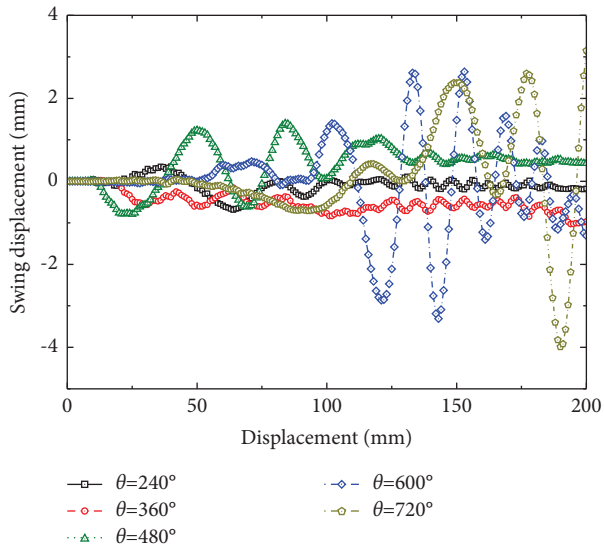

Figure 12: *X*-direction swing displacement diagram of members with different torsion angles.

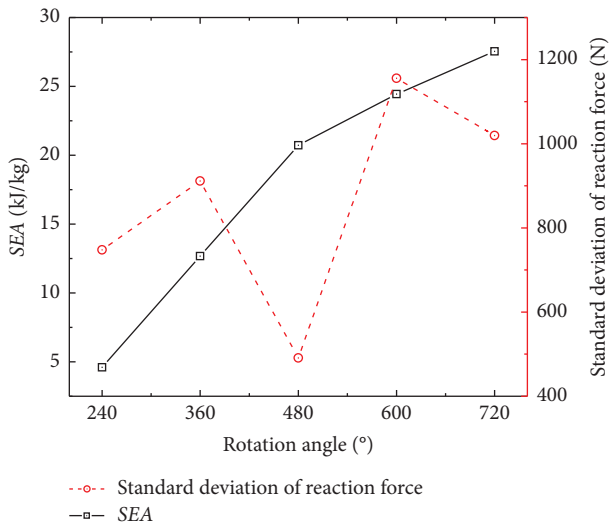

Figure 13: σ-*SEA* curve of members with different torsion angles.

trend, when the torsion angle is small, the torsion plate member did not occur completely plastic deformation, it is part of the region of elastic deformation of the branch reaction force will produce small fluctuations in the phenomenon, increasing its standard deviation. When the torsion angle is between 360° and 600°, the energy-absorbing member has undergone good plastic deformation and has not produced an elastic recovery phenomenon, so the platform reaction force is more stable in this range. When the torsion angle exceeds 600°, due to the increase of F_N, the torsion plate has obvious scratches and swing yielding phenomenon, resulting in obvious swinging phenomenon of the reaction force, and the standard deviation has a larger value up to 1155.6 N, which affects the smoothness of energy absorption.

As shown in Figure 14 is the tensile length and the length of the reaction platform stage graph. It can be seen from the figure, with the increase of the torsion angle, the clamping

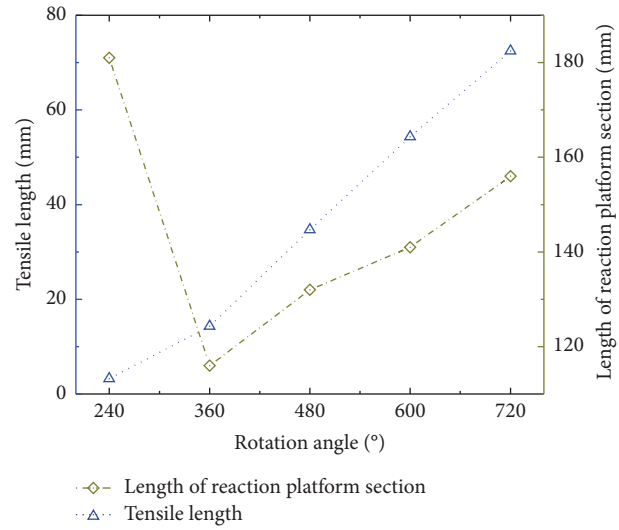

Figure 14: Δl-*s* curve of members with different torsion angles.

angle between the pressure plate and the torsion plate is increasing, and the compressive stress perpendicular to the direction of the torsion plate is higher. As the friction coefficient is certain, the downward tensile stress of the torsion plate under the influence of friction gradually increases. In the process of plastic deformation of the torsion plate, the torsion plate also undergoes axial tensile deformation, and the tensile length increases linearly with the rotation angle of the torsion plate. The tensile lengths under the five conditions are 3.24 mm, 14.33 mm, 34.68 mm, 54.35 mm, and 72.44 mm, respectively. The occurrence of this stretching phenomenon is not favourable for the energy absorption of the energy-absorbing members. As the tensile stress increases, the torsion plate will appear to be pulled off, so the occurrence of the tensile phenomenon should be minimised. When the torsion angle is 240°, the torsion plate is only in the boundary of plastic deformation, most of the torsion plate internal elastic deformation, so the torsion plate of the platform reaction force for the elastic force to support, the reaction force is smaller, through the reaction force peak point directly into the platform stage. With the increase of the torsion angle, the torsion plate undergoes plastic deformation in more areas, and there are four obvious stages of the elasticity-yield-climbing-platform in the torsion process. The distance to reach the platform stage gradually decreases, so the length of the counterforce platform gradually increases, and the length of the counterforce platform between the torsion angles of 360°~720° are 116 mm, 132 mm, 141 mm, and 156 mm. The increase in the length of the counterforce platform can effectively increase the energy absorption capacity and enhance the effect of the anti-impact energy absorption.

5.2. Effect of Plate Thickness on Impact Energy Absorption Characteristics. Under the conditions of impact velocity of 4 m/s, total length of 200 mm, torsion angles of 480°, and fillet radius of 3 mm, the simulation studies were carried out for plates thicknesses of 3 mm, 4 mm, 5 mm, 6 mm, and

7 mm. Figure 15 shows the stress cloud of the energy-absorbing member under different plate thicknesses with 200 mm displacement of the pressure plate. From the figure, it can be seen that in the process of moving down the pressure plate, the torsion plate and the pressure plate contact location are obvious plastic deformation. When the plate thickness is thin, its torsion radius is large and the bearing capacity is low. After the deformation of the torsion plate, there is an elastic recovery phenomenon so that the flatness of the structural components is reduced, and the swing phenomenon of the overall plate appears. As the plate thickness increases, the flatness of the plate is improved, but it is more likely to appear in the stage of the scratch phenomenon, and the width of the scratch gradually increases. Its torsional moment gradually decreases, so the force required to provide deformation increases, resulting in a larger plastic deformation region, the higher the flatness. When the yield phenomenon occurs, a unilateral scratch buildup occurs, causing an increase in stress. The plate affected by the stress appears to swing, and the reciprocating motion appears to stage the scratch phenomenon. There is a certain inherent frequency of this phenomenon, which is not conducive to anti-impact energy absorption.

As shown in Figure 16, the reaction force-displacement curves of energy-absorbing members under different plate thicknesses are presented. From the figure, it can be seen that each energy-absorbing member has obvious elastic deformation stage, yield deformation stage, reaction force raising stage, and platform stage. Each torsion plate has no obvious peak pressure point and resistance drop process, and the platform stage is long and smooth. With the increase of plate thickness, the reaction force increases continuously, the mean values of reaction force under five thicknesses are 22.37 kN, 30.82 kN, 40.58 kN, 55.66 kN, and 66.32 kN, and they enter into the platform stage at a similar position. The constant force effect of the reaction platform stage is stable when the plate thickness is 5 mm and below, there is no obvious fluctuation phenomenon; when the plate thickness is 6 mm and 7 mm, the contact space between the pressure plate and the torsion plate is small due to the increase of plate thickness. Compared with the smaller thickness condition, the contact position is more advanced when the plate thickness increases. In the case of the same displacement, the thick plate deformation is greater, from the position of the contact point scratch phenomenon is particularly obvious, and the scratch width is large, energy-absorbing members are more easily to appear in the stage of the scratch phenomenon so that there are reaction force fluctuations. When the plate thickness is 7 mm, the fluctuation phenomenon is obvious at the stage of reaction force climbing. As shown in Figure 17, the energy absorption curves of the members with different plate thicknesses, the final energy absorption of the five members are 4.48 kJ, 6.18 kJ, 8.13 kJ, 11.16 kJ, and 13.29 kJ. The energy of each member in the elasticity-yield-climbing stage grows slowly, and it shows a linear growth trend after entering the platform stage of the reaction force. The plate thicknesses of 6 mm and 7 mm show the fluctuation phenomenon of reaction force, but the fluctuation amplitude is small, so it has less influence on the energy absorption, and the energy absorption effect of each group of components is stable.

As shown in Figure 18 for different plate thickness conditions under the torsion of the lower end of the plate centre point position change. When the plate thickness is 5 mm, the swing of the plate is small in the process of moving down, the maximum swing displacement in the width direction is 1.11 mm, the maximum swing displacement in the length direction is 1.38 mm, and the deformation of the plate is more stable; when the plate thickness increases or decreases, the plate has an obvious swinging phenomenon, of which the swinging phenomenon is the most significant when the plate thickness is 7 mm, the maximum swinging displacement in the width direction is 11.14 mm, and the maximum swinging displacement in the length direction is 4.36 mm. The change of plate thickness has a greater effect on the swing amplitude of the plate, but it has a smaller effect on its swing frequency.

As shown in Figure 19 for different plate thickness conditions of the standard deviation of reaction force and the *SEA* curves. It can be seen from the figure, with the increase of plate thickness, the *SEA* shows a gradual increase in the trend. When the plate thickness is less than 5 mm, the *SEA* shows a linear growth trend, and when the plate thickness is 6 mm, the *SEA* growth rate first accelerates and then slows down. The *SEAs* of five energy-absorbing members are 19.03 kJ/kg, 19.67 kJ/kg, 20.72 J/kg, 23.68 J/kg, and 24.19 J/kg. When the plate thickness is small, the platform reaction force swing phenomenon is not significant, its standard deviation value is low, and the support reaction force stabilisation effect is good. The plate thickness increases to 6 mm and above, the torsion plate stage scratch phenomenon makes the reaction force fluctuation phenomenon, the standard deviation of the reaction force in the plate thickness of 6 mm when the maximum value of 927.74 N, proving that the support reaction force fluctuation phenomenon is the most significant under this condition.

The torsion plate tensile length and the length of reaction platform stage are shown in Figure 20. Both the tensile length and the reaction platform length increase with the increase in plate thickness. Tensile length increased from 31.60 mm to 38.07 mm, due to the increase in scratch width, the torsion radius decreases, the F_N increases so that the friction increases, the torsion plate radial tensile stress increases. At this time, the positive tensile stress of the torsion plate is greater than its tensile strength so that the torsion plate is elongated by the tensile, but it does not exceed its tensile limit. With the increase of plate thickness, the bearing capacity of the energy-absorbing member is increased, and the more forward the yield deformation position of the member is, the faster the members reach the stage of the reaction platform, and its reaction platform length increases. The length of the reaction platform stage under each condition is 127 mm, 130 mm, 132 mm, 132 mm, and 135 mm. It can be seen that although there is a tendency for the reaction plateau length to increase, the change in this magnitude is small, and the change in the plate thickness condition has little effect on the reaction platform length.

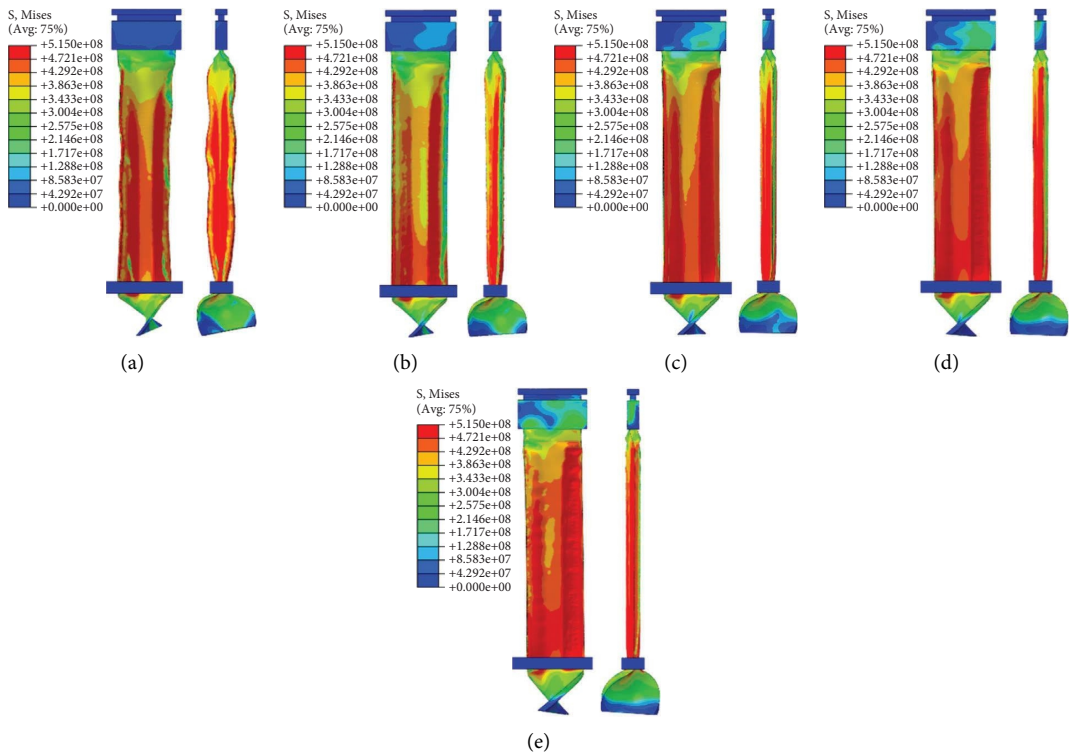

Figure 15: Stress cloud diagram of components with different plate thicknesses. (a) $b = 3$ mm. (b) $b = 4$ mm. (c) $b = 5$ mm. (d) $b = 6$ mm. (e) $b = 7$ mm.

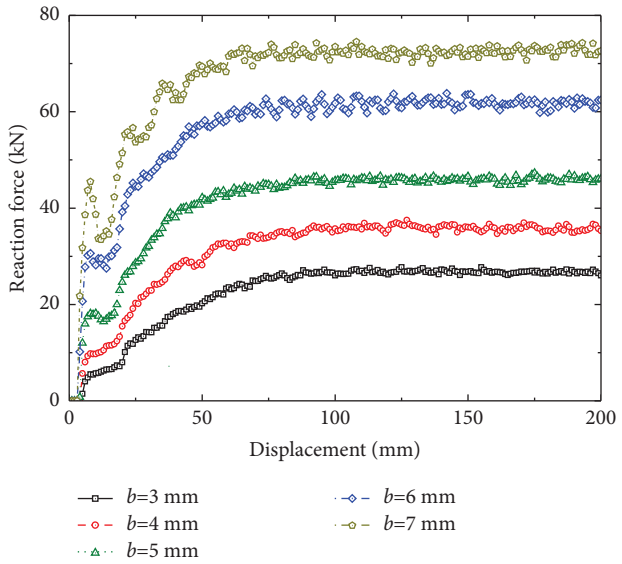

Figure 16: Reaction force-displacement curves of members with different plate thicknesses.

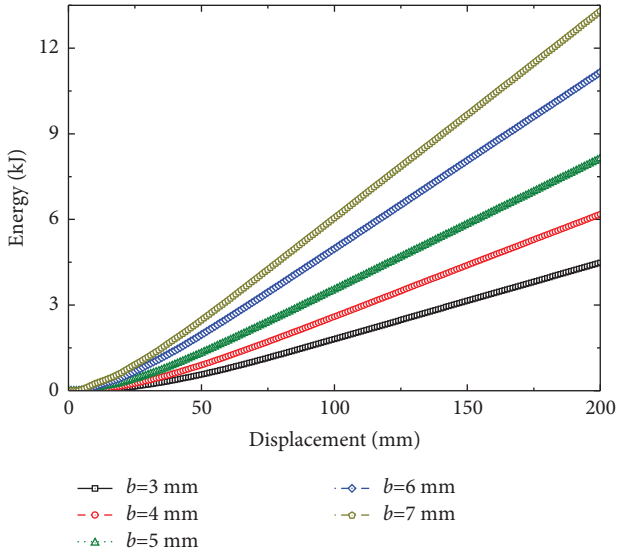

Figure 17: Energy absorption characteristic curves of members with different plate thicknesses.

5.3. Effect of Fillet Radius on Impact Energy Absorption Characteristics. Under the conditions of impact velocity of 4 m/s, total length of 200 mm, plate thickness of 5 mm, and torsion angles of 480°, the simulation studies were carried out for the fillet radii of 2 mm, 2.5 mm, 3 mm, 3.5 mm, and 4 mm. As shown in Figure 21, the stress cloud of the energy-absorbing member is shown when the displacement of the plate is 200 mm under the condition of different fillet radii. From the figure, it can be seen that the plate has high flatness, and there is no torsional recovery phenomenon. The plastic deformation of the torsion plate is obvious in the deformation process. When the fillet radius is 2 mm, the plate appears as obvious corrugation in the deformation process. As the gap between the pressure plate and the torsion plate is small, the closer its contact point is to the centre line of the torsion plate. The decrease in the radius of the torsion makes

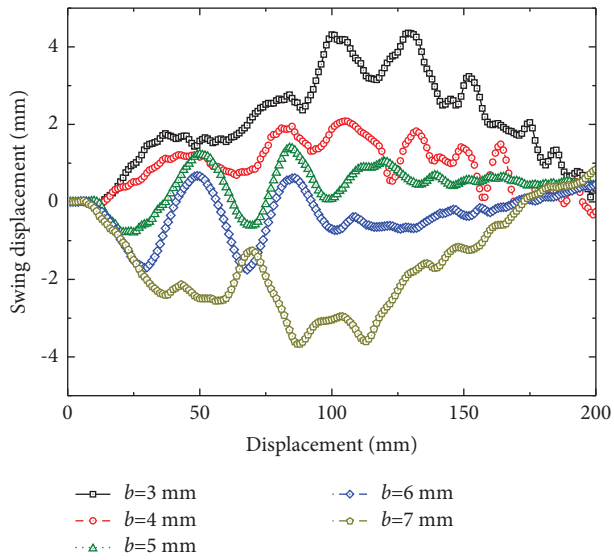

Figure 18: X-direction swing displacement diagram with different plate thickness.

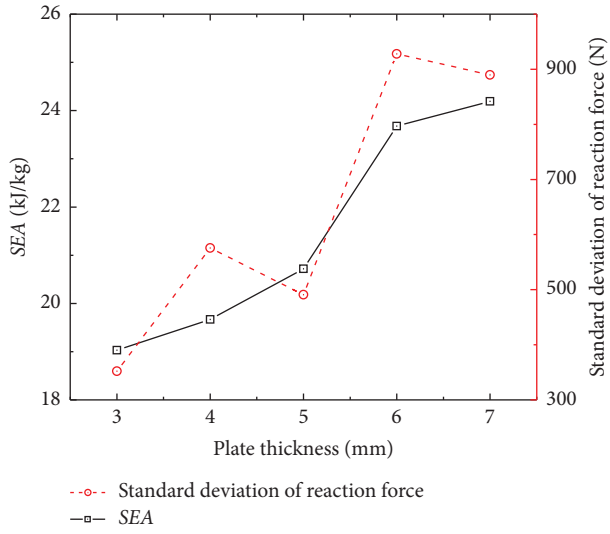

Figure 19: σ-SEA curve with different plate thickness.

the F_N increase, and it will have obvious stress concentration within the unit deformation range, resulting in the accumulation of scratches so that the torsion plate begins to swing to give way to the corrugated shape. With the increase of the fillet radius, the pressure plate and the torsion plate clearance increases, the torsion radius increases so that the F_N decreases, the stress concentration phenomenon slows down, and the periodic scratch phenomenon is weakened. When the radius of the corner is larger than 3 mm, there is no obvious scratch fluctuation phenomenon, the scratch is continuous and regular, and in the overall deformation process of the torsion plate, stress is reduced.

The force-displacement curves of the energy-absorbing members under different fillet radius conditions are shown in Figure 22. From the figure, it can be seen that each energy-absorbing member presents obvious elastic deformation stage, yield deformation stage, reaction force raising stage,

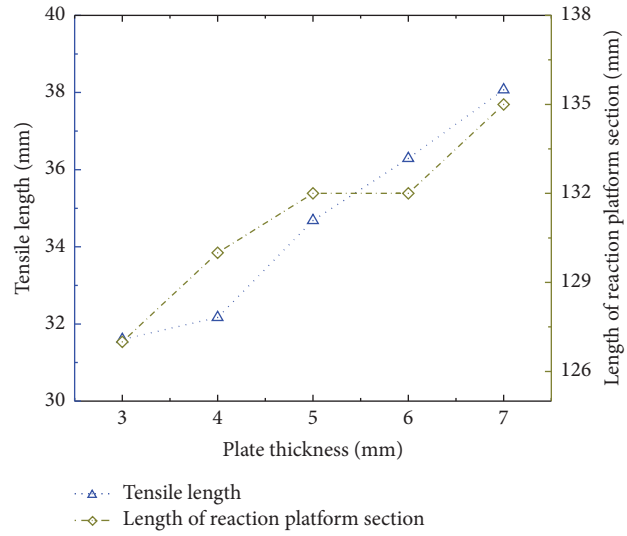

Figure 20: Δl-s curve with different plate thickness.

and platform stage, and the five members have the same trend of change. Their mean values of reaction force are 44.31 kN, 45.39 kN, 40.58 kN, 40.47 kN, and 38.88 kN, in which the mean values of reaction force under the three conditions of $r = 3$ mm, 3.5 mm, and 4 mm are similar, and the positions of entering into the platform stage are similar. The platform stage of the reaction force does not have obvious fluctuation of reaction force, and the change of reaction force is smooth. As the radius of the corner decreases, the torsional radius decreases, the torsional force F_N increases, and the reaction force increases, but the reaction force does not grow linearly. $r = 2.5$ mm when the mean value of reaction force is greater than the mean value of reaction force when $r = 2$ mm, the reason is that $r = 2$ mm due to the stress buildup produced by the torsion of the torsion plate swinging to give way to make the reaction force is unstable, and the fluctuation phenomenon is obvious. Although its peak point of reaction force is higher, the overall mean load is reduced. The energy absorption curves of the energy-absorbing members with different fillet radii are shown in Figure 23. As can be seen from the figure, the final energy absorption of the five components is 8.88 kJ, 9.10 kJ, 8.13 kJ, 8.11 kJ, and 7.79 kJ. When the radius of the fillet is 3~4 mm, the deformation of torsion plate is stable, the absorption energy is similar, and with the decrease of the fillet radius, the absorption energy is slightly increased; when the radius of the fillet is 2 mm, the absorption energy is slightly lower than that of 2.5 mm, which is mainly due to the fluctuation of the reaction force in the process of deformation, which results in the reduction of the support reaction force, and the growth tendency of the reaction force is slowed down in the reaction force plateau stage. Therefore, with the increase of the radius of the fillet, the absorption energy shows the trend of increasing and then decreasing.

As can be seen in Figure 24, with the increase of the fillet radius, the swing phenomenon of the member in the process of energy absorption is obviously slowed down, and the swing amplitude is gradually reduced, in which the swing

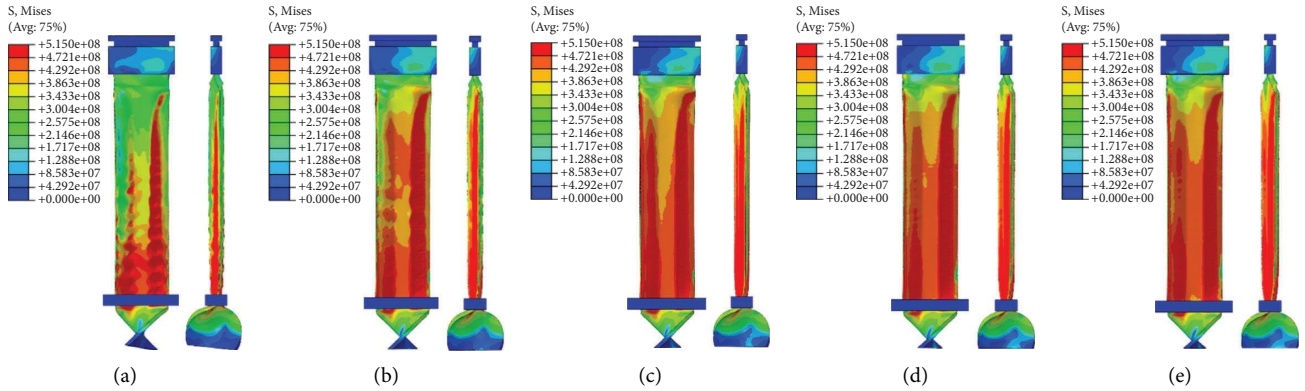

Figure 21: Stress cloud diagram of different pressure plate fillet radius members. (a) $r = 2$ mm. (b) $r = 2.5$ mm. (c) $r = 3$ mm. (d) $r = 3.5$ mm. (e) $r = 4$ mm.

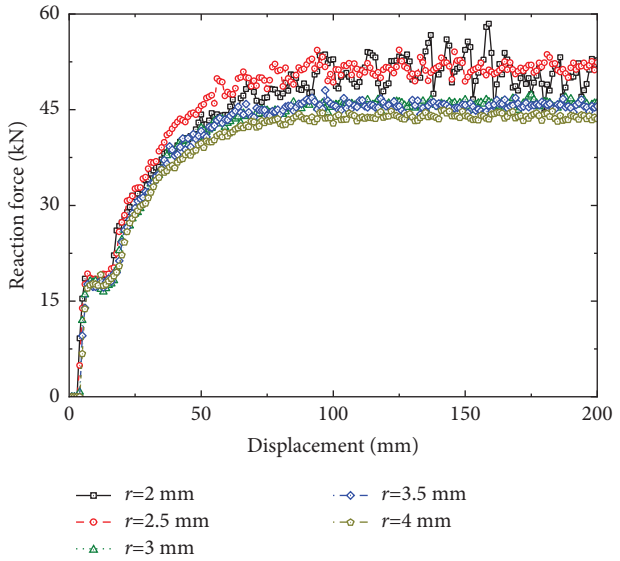

Figure 22: Reaction force-displacement curve of different pressure plate fillet members.

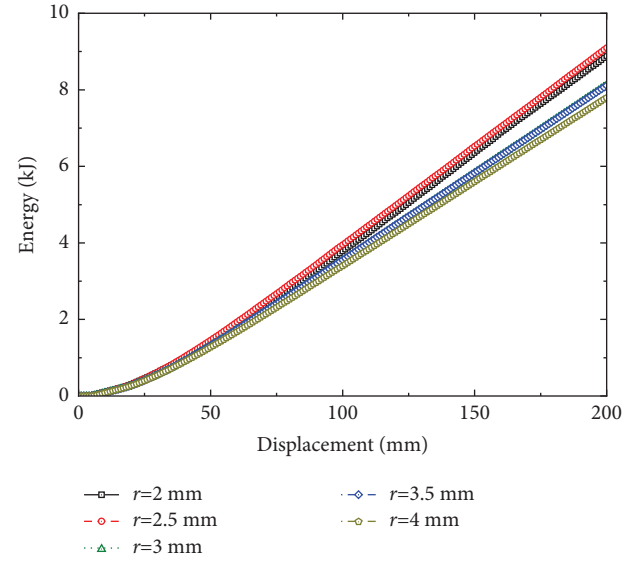

Figure 23: Energy absorption characteristic curve of different pressure plate fillet members.

amplitude is the largest under the condition of 2 mm, ranging from −5.08 mm to 4.68 mm, and the maximum distance is 9.76 mm; the swing amplitude is the smallest under the condition of 4 mm, ranging from 0 mm to 1.40 mm, and the maximum distance is 1.40 mm. With the increase of the fillet radius, it can effectively alleviate the phenomenon of torsion plate fluctuation, but at the same time, the support reaction force will be reduced.

The standard deviation of reaction force and *SEA* curves under different fillet radius conditions are shown in Figure 25. With the increase of the fillet radius, the *SEAs* of the five members are 22.64 kJ/kg, 23.18 kJ/kg, 20.72 J/kg, 20.67 J/kg, and 19.86 J/kg. The *SEA* shows the trend of increasing and then decreasing, and its trend is consistent with the trend of energy change. When the fillet radius is 2 mm, the *SEA* is reduced due to the fluctuation phenomenon of the reaction force; the fillet radius is 2.5~4 mm, with the increase of the fillet radius, the *SEA* decreases linearly; the standard deviation of the fillet radius is linearly reduced within the range of 2~3 mm, in which the fluctuation is most significant under the condition of 2 mm, with the standard deviation of 2616.9 N; when the fillet radius is 3~4 mm, the *SEA* decreases linearly due to the increase of the fillet radius. When the fillet radius is in the range of 3~4 mm, the plastic deformation of the torsion plate is smooth and the fluctuation of the reaction force is small, with similar standard deviation values of 490.8 N, 603.0 N, and 433.0 N, which are small and the energy-absorbing effect is stable.

The tensile length and the length of the reaction platform stage under the change of the fillet radius condition are shown in Figure 26. The tensile length tends to decrease linearly with the increase of the fillet radius. The torsion plate extension is due to the axial tensile load on the torsion plate during the downward movement of the plate. The mean value of the reaction force under the condition of 2 mm fillet radius is smaller than the mean value of the reaction force under the condition of 2.5 mm, but the tensile length is opposite to the trend of the reaction force, with the tensile

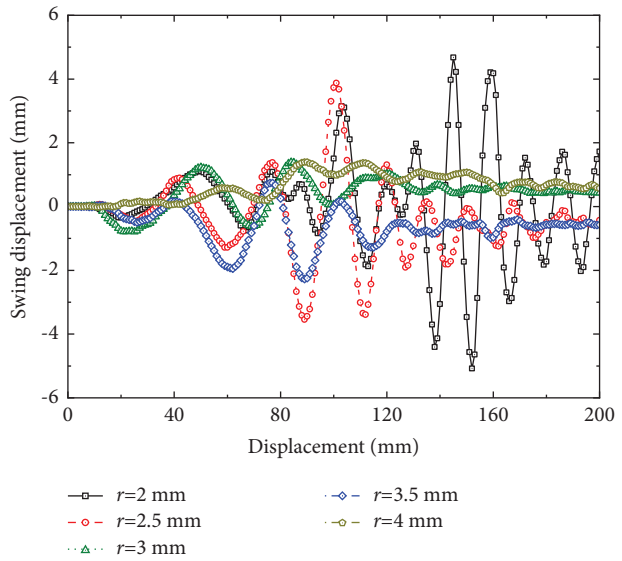

Figure 24: X-direction swing displacement diagram with different fillet radius.

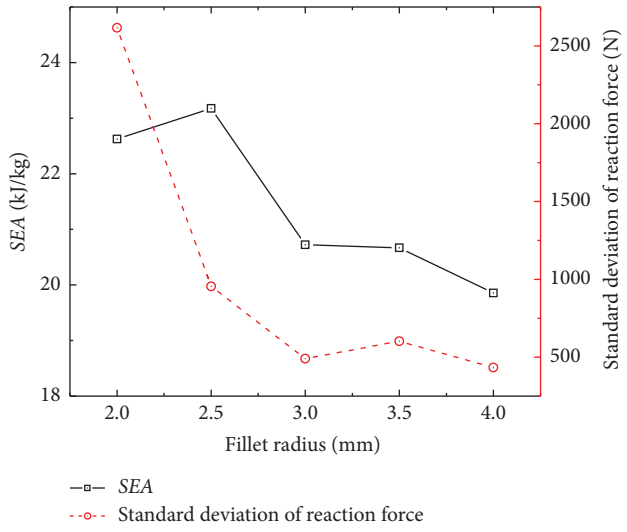

Figure 25: σ-SEA curve with different fillet radius.

lengths of 38.2 mm at 2 mm and 36.13 mm at 2.5 mm. The reason for this is that the stress concentration phenomenon of the torsion plate will continuously occur during the energy absorption process under the 2 mm condition, and the peak point of the counterforce will continuously occur, the frequency and value of which are greater than the result of 2.5 mm, which results in the staged stretching of the torsion plate, and the total amount of which is ultimately greater than that of the total amount of the stretching of 2.5 mm. When the fillet radius is greater than 2.5 mm, the phenomenon does not appear, and its trend is the same as the trend of the mean value of the reaction force. When the fillet radius is less than 3 mm, the length of the reaction force platform stage increases with the increase of the fillet radius, and due to its significant fluctuation phenomenon and the high value of the reaction force, the time to reach a stable platform stage increases. When the fillet radius is larger than

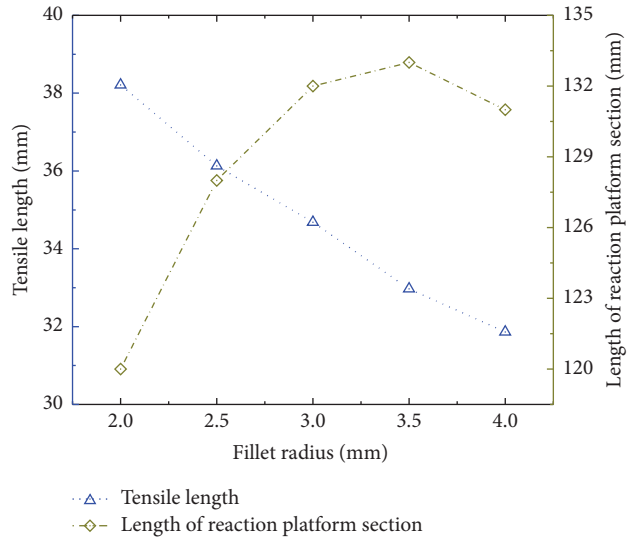

Figure 26: Δl-s curve with different fillet radius.

3 mm, the fluctuation phenomenon gradually disappears, and the mean value of the torsion plate reaction force of each group is similar, so it enters the similar position of the reaction platform stage, and the length of the reaction platform stage is about 132 mm. So, the smaller corner radius has a greater effect on the length of the reaction platform stage, and with the increase of the fillet radius, the fillet radius has no significant effect on the length of the reaction platform stage.

6. Conclusion

A torsion plate energy-absorbing member was designed, and its energy-absorbing and anti-impact characteristics were simulated and analysed, leading to the following conclusions.

(1) The torsion plate energy-absorbing member is deformation stable. It has good repeatability and controllability. The energy-absorbing member has four stages of action: elastic stage, yield stage, reaction force rising stage, and reaction force platform stage, and the member has high flatness after deformation. The travelling efficiency of the member can reach 100%.

(2) With the increase of the torsion angle, the flatness of the torsion plate increases and there is a phenomenon of increasing the plastic deformation zone and rising the support reaction force. The torsion plate produces a phenomenon of stage scratching and inward contraction. The phenomenon of torsion plate swing becomes more and more significant. All of its energies were linearly increased, while the SEA gradually increased, but the trend slowed down. The standard deviation reaches its minimum at 480°. The tensile length of each member and the length of the reaction platform gradually increased.

(3) Plate thickness value is too large or too small and will affect the flattening effect of the torsion plate. As the

plate thickness increases, the reaction force increases and produces the phenomenon of stage scratches. The oscillation of the torsion plate becomes more and more obvious, and the maximum oscillation displacement is 11.14 mm when the plate thickness is 7 mm. The *SEA* gradually increases. The standard deviation reaches the peak point at 6 mm. The torsion plate tensile length and the reaction platform length are increasing.

(4) With the increase of the fillet radius, the flatness of the plate is increased. The mean load shows a trend of increasing and then decreasing. The mean value of the reaction force reaches the maximum when the fillet radius is 2.5 mm. The fluctuation phenomenon of the torsion plate under the condition of 2 mm is the most significant. The fluctuation phenomenon of the reaction force is obvious. The *SEA* has the same trend with the mean load trend. The plate tensile length decreases continuously and gradually with the increase of the fillet radius, and the force reaction platform stage increases linearly within 2~3 mm, and the values are similar in 3~4 mm.

(5) The torsion plate energy-absorbing member is a kind of ideal energy-absorbing and anti-impact member, which has many advantages such as small volume, convenient processing, easy to replace, and so on. According to the support needs of the plate for different parameters of processing and different number of combinations, it can be used in combination with conventional columns to effectively enhance the column's impact performance and protect the column.

Data Availability

Some or all data, models, or codes generated or used during the study are available from the corresponding authors upon request.

Conflicts of Interest

The authors declare that there are no conflicts of interest regarding the publication of this paper.

Acknowledgments

The writing of this paper was funded by several foundation projects, including: National Natural Science Foundation of China-Research on the theory and method of design of adaptive anti-impact roadway hydraulic support for impacted ground pressure mines; National Key Research and Development Program of China-Intelligent impact support technology and equipment for impact hazardous roadways and engineering demonstration; National Natural Science Foundation of China-Research project on the mechanism of energy absorption and anti-scouring and its memory effect of impacted ground pressure coal seam borehole group; Liaoning Provincial Science and Technology Department Project-Research on the mechanism of cooperative support of three-stage support equipment for roadway.

References

[1] Y. S. Pan, *Rock Burst of Coal Mine*, Science Press, Beijing, China, 2018.

[2] G. F. Wang, Q. Li, Z. L. Zhao, and Y. Pang, "The impact tendentiousness testing of working faces and roadways with strong rock burst and fore support system," *Journal of Shandong University of Science and Technology*, vol. 30, no. 4, pp. 1–9, 2011.

[3] Q. X. Qi, Y. S. Pan, H. T. Li et al., "Theoretical basis and key technology of prevention and control of coal-rock dynamic disasters in deep coal mining," *Journal of China Coal Society*, vol. 45, no. 5, pp. 1567–1584, 2020.

[4] F. Q. Ren, C. Zhu, M. C. He, J. Shang, G. Feng, and J. Bai, "Characteristics and precursor of static and dynamic triggered rockburst: insight from multifractal," *Rock Mechanics and Rock Engineering*, vol. 56, no. 3, pp. 1945–1967, 2022.

[5] H. P. Kang, Y. Z. Wu, J. He, and Y. K. Fu, "Rock bolting performance and field practice in deep roadway with rock burst," *Journal of China Coal Society*, vol. 40, no. 10, pp. 2225–2233, 2015.

[6] M. C. He, Q. R. Sui, M. N. Li, Z. Wang, and Z. Tao, "Compensation excavation method control for large deformation disaster of mountain soft rock tunnel," *International Journal of Mining Science and Technology*, vol. 32, no. 5, pp. 951–963, 2022.

[7] M. C. He, H. P. Xie, S. P. Peng, and Y. D. Jiang, "Study on rock mechanics in deep mining engineering," *Chinese Journal of Rock Mechanics and Engineering*, vol. 24, no. 16, pp. 2803–2813, 2005.

[8] Q. Wang, S. Xu, Z. X. Xin, M. He, H. Wei, and B. Jiang, "Mechanical properties and field application of constant resistance energy-absorbing anchor cable," *Tunnelling and Underground Space Technology*, vol. 125, Article ID 104526, 2022.

[9] Y. S. Pan, Y. H. Xiao, Z. H. Li, and K. X. Wang, "Study of tunnel support theory of rock burst in coal mine and its application," *Journal of China Coal Society*, vol. 39, no. 2, pp. 222–228, 2014.

[10] X. S. Dai and J. M. Ma, "Energy absorbed by a metal tube under axial crush load," *Journal of Vibration and Shock*, vol. 31, no. 06, pp. 100–103+125, 2012.

[11] Z. Tang, H. Y. Fu, and J. Wang, "Energy absorption characteristics of hexagonal thin-plateed component under quasi-static radial compression," *Chinese Journal of Underground Space and Engineering*, vol. 14, no. 01, pp. 72–77, 2018.

[12] C. H. Wang, D. An, and C. Han, "Simulation and tests for new tubular type energy-absorbing and anti-impact members with stiffened plate under rock burst," *Journal of Vibration and Shock*, vol. 38, no. 11, pp. 203–210+241, 2019.

[13] C. J. Luo, R. Q. Liu, Z. Q. Deng, M. Li, and J. J. Shen, "Experimental investigations of an energy absorber based on thin-plateed metal tube's plastic deformation," *Journal of Vibration and Shock*, vol. 29, no. 04, pp. 101–106+234, 2010.

[14] Y. H. Xiao, Y. S. Pan, and J. Q. Chen, "Buckling energy absorption reliability of energy absorption component of roadway rockburst preventing support," *Journal of Mining & Safety Engineering*, vol. 39, no. 02, pp. 317–327, 2022.

[15] J. Z. Zhang, H. Liu, and J. Wang, "Design and energy-absorbing properties of the everting components of straight

corrugated tubes," *Journal of Vibration and Shock*, vol. 39, no. 9, pp. 49–56, 2020.

[16] C. Qi, F. L. Dong, S. Yang, and W. Dong, "Energy-absorbing characteristics of a tapered multi-cell thin-plateed tube under oblique impact," *Journal of Vibration and Shock*, vol. 31, no. 24, pp. 102–107, 2012.

[17] Y. U. Tong-xi and L. U. Guo-xing, *Energy Absorption of Structures and Materials*, Chemical Industry Press, Beijing, China, 2005.

[18] W. Nie, W. Wang, Z. Tao, C. Zhu, and Y. Chen, "Numerical modeling of the NPR-cable and its applications for analysis of a slide-toe-toppling failure," *Computers and Geotechnics*, vol. 149, Article ID 104852, 2022.

[19] D. Blanchard and G. Griso, "Asymptotic behavior of a structure made by a plate and a straight rod," *Chinese Annals of Mathematics, Series B*, vol. 34, 2013.

[20] F. Brezzi, J. A. Evans, T. Hughes, and L. Marini, "New rectangular plate elements based on twist-Kirchhoff theory," *Computer Methods in Applied Mechanics and Engineering*, vol. 200, no. 33-36, pp. 2547–2561, 2011.

[21] H. Y. Yu, J. H. Wu, and R. P. Li, "Discussion on elastic free torsion of rectangular bar," *Mechanics and Practice*, vol. 02, pp. 73-74, 2007.

[22] W. G. Long and B. Jin, "Discussion on the material mechanics method of free torsion of long and narrow rectangular cross section bar," *Mechanics and Practice*, vol. 2, pp. 60-61, 2003.

[23] S. Tang, J. Li, S. Ding, and L. Zhang, "The influence of water-stress loading sequences on the creep behavior of granite," *Bulletin of Engineering Geology and the Environment*, vol. 81, no. 11, pp. 482–515, 2022.

[24] E. Anderheggen, "A conforming triangular finite element plate bending solution," *International Journal for Numerical Methods in Engineering*, vol. 2, no. 2, pp. 259–264, 1970.